UNIVERSITY OF CALIFORNIA SAN DIEGO

Laser-Induced-Graphene on Metal Substrate for Capacitive De-ionization

A Thesis submitted in partial satisfaction of the requirements
for the degree Master of Science

in

Nanoengineering

by

Fatih Aybar

Committee in charge:

Professor Sadik Esener, Chair
Professor Michael Heller, Co-Chair
Professor Shaochen Chen

2021

The thesis of Fatih Aybar is approved, and it is acceptable in quality and form for publication on microfilm and electronically.

University of California San Diego

2021

DEDICATION

I would like to acknowledge the scientific community for advancing knowledge and technology, vaccines for diseases, solutions for peace and prosperity for all. Thank you to University of California, San Diego for a chance to make a contribution and thanks to my family for patience and support.

TABLE OF CONTENTS

LIST OF FIGURES

LIST OF TABLES

ABSTRACT OF THE THESIS

Laser-Induced-Graphene on Metal Substrate for Capacitive De-ionization

by

Fatih Aybar

Master of Science in Nanoengineering

University of California San Diego, 2021

Professor Sadik Esener, Chair
Professor Michael Heller, Co-Chair

The Earth has an abundance of seawater but sources of fresh water for domestic use, agriculture or industry make up only 2.5% of this natural resource. The method of capacitive deionization (CDI) can desalinate water more efficiently than reverse osmosis at low salt concentration or brackish water. Electrodes and material binders directly affect CDI performance and efficiency. In order to mass produce electrodes with increased CDI

efficiency, a low-cost manufacturing method of forming laser-induced-graphene (LIG) directly on a polyimide spin-coated metal substrate disclosed. CDI efficiency improvement is analyzed for the electrodes manufactured with this method. The application of this technology for brackish water desalination is tested. Potential capability of electrode refurbishing against bio-fouling is also discussed.

Chapter 1

Desalination

1.1 Motivation

For human survival on planet earth, people need energy, water and food. The sun is the biggest source of energy in our solar system and we have a sustainable way of utilizing a portion of this energy by solar energy generation methods. Water and food on the other hand are linked to natural resources but can be attained using energy. Even though 70% of the surface of our planet is covered by the natural resource of water, it is high in salt content which is not directly usable for drinking, irrigation or industrial use. Sources of fresh water are much more limited and make up only a small percentage at 2.5%[1]. Fresh water is also becoming a scarce resource due to population growth, global industrialization and climate change; hence desalination of seawater is essential to support the future of humanity.

1.2 Desalination

Desalination of seawater requires a great amount of energy. As the most common high volume water desalination method, reverse osmosis (RO) still requires around 3kWh of energy per m^3 of water[2]. For perspective, this energy is the equivalent of driving about 12.5 miles in an electric vehicle or continuously running a typical kitchen microwave

oven for 3 hours. Other desalination methods exist such as thermal evaporation, electrodialysis, and capacitive deionization but only capacitive deionization (CDI) shows potential as an energy efficient alternative to RO at low ion concentration levels[3]. However, multiple challenges remain for CDI to be a competitive alternative to RO desalination, some of which this thesis will focus on advancing.

1.3 Capacitive Deionization

Capacitive deionization is electrosorption of ions by a potential difference between high surface area electrodes. As electrodes are charged, an electric double layer (EDL) forms on the surface of electrode material where ions are either adsorbed or desorbed from the saline solution. For high surface area electrode materials, this EDL on electrode-liquid interfaces create a highly capacitive electronic device. Charging and discharging of electrode is controlled by the applied voltage across electrodes and this enables the following: (1) fine control over energy consumption at low pressure in contrast to high pressures needed in RO and (2) the possibility of energy recovery by capturing energy stored in this EDL capacitance.

The operation of CDI is similar to EDL capacitors or supercapacitors however the liquid electrolyte material is a saline solution which is held then pumped across the electrodes during operation whereas energy storage devices maintain and use the same electrolyte. Common with energy storage devices, CDI performance is highly dependent on electrode properties.

Electrodes with high surface area and low tortuosity are critical for CDI performance since solidum and chloride ions accumulate near the electrode surface. There have been many materials analyzed, evaluated or created for the purpose of CDI such as activated carbon (AC), carbon nano-tubes, carbon aerogels[2]. There are advantages and disadvantages to each material studied for CDI. Activated carbon can provide high surface at low cost but AC is prone to bio-fouling and faradaic reactions[2]. Forests of carbon nano-tubes can enable fine control of surface area and although roll to toll CVD processes have been reported[4], CVD process is still expensive when compared to manufacture of other electrode materials for CDI such as laser induced graphene. Laser-power generated graphene electrodes can provide high surface with control over surface morphology but this manufacturing method too must be prepared for industrial use. The electrical interface between the high surface are materials and metal current collectors must be as low as possible to increase efficiency of CDI. This thesis discloses a method to generate high surface area graphene material with nano-meter features and apply it onto a metal substrate with low resistance to increase CDI efficiency. Other potential benefits and improvements will also be discussed to bring graphene closer to industrial use in desalination.

1.4 Challenges for CDI

Capacitive deionization (CDI) is a more energy efficient alternative to RO for brackish water concentration, with energy use of around 0.2 kW/m^3 for CDI[2]. Since the first investigation in CDI technology from 1960s, there has been progress made in

improving CDI, yet several challenges remain to scale CDI into a commercially feasible alternative to RO:

1. Scalable electrode material manufacturing
2. Ease of system assembly into a stack of cells
3. Energy recovery and overall efficiency
4. Scaling and Bio-fouling.

The first challenge has multiple requirements to be met on its own. For example, electro-sorption capacity for ions, high conductivity, resilience against bio-fouling, chemical stability and the ability to be tuned for the application. The second challenge focuses on system level engineering to scale a prototype into a viable commercial solution and for ease of operation and maintenance. Solutions to these challenges are important for CDI based technologies to have a significant impact in addressing the problem of water scarcity. A viable CDI solution is a system which addresses all these challenges in a scalable, low-cost manner. If the efficiency of CDI can be improved, it can provide a low cost, small form-factor desalination option that is portable and can be distributed to many parts of the world as an appliance without big investments needed for a city-wide desalination solution such as RO.

Multiple efforts are being explored for reducing the energy consumption of CDI such as membrane enhance capacitive desalination (M-CDI) and energy recovery. Although research has been done to understand CDI electrodes in detail[3,5,6], this work aims to advance efficiency by lowering electrode active material and metal current collector electrical resistance in order to increase efficiency of CDI.

1.5 Thesis Contribution

In this work, the models for this interface are discussed and a method of manufacturing is disclosed to form laser induced graphene directly on a metal current collector substrate. Current collector is herein referred to as substrate because the electrode active material is manufactured formed directly on the metal surface.

A low cost, scalable manufacturing method that enables improved electrode efficiency by the innovation of forming laser-induced-graphene (LIG) on a metal substrate is disclosed. The application of this technology for brackish water desalination is tested. Formation of graphene on a metal substrate can also be utilized for other purposes such as for supercapacitors or batteries.

As a secondary benefit left to be explored is that creating LIG directly on a metal substrate also enables the possibility of electrode reconditioning by re-application of the same laser manufacturing method to ablate bio-fouling deposits and turn them into graphene as well. Study of turning bio-materials into graphene is out of scope of this work and this potential with prior work will be discussed.

Chapter 2

CDI System

2.1 Introduction

Capacitive deionization (CDI) is the removal of ions from a dissolved salt aqueous solution via charging and discharging of electrodes that absorb and desorb excess ions. As a potential difference is applied across the electrodes in the solution, ions are pulled to the solid-liquid interface of the electrodes. Positive ions such as Na+ cations are electro-absorbed to the negative electrode and similarly, negatively charged anions such as Cl- to the positively charged electrode. Electrodes are discharged by lowering the potential difference to zero, and the ions are then desorbed back into the solution. Since saline solutions conduct electricity, a separator material is necessary in between the electrodes. A basic CDI cell and a CDI desalination stack made up of multiple cells in series are shown in Figure 1 on the left and right respectively. As the solution flows through the stack (coils though in this example), ion concentration is further reduced passing through each cell.

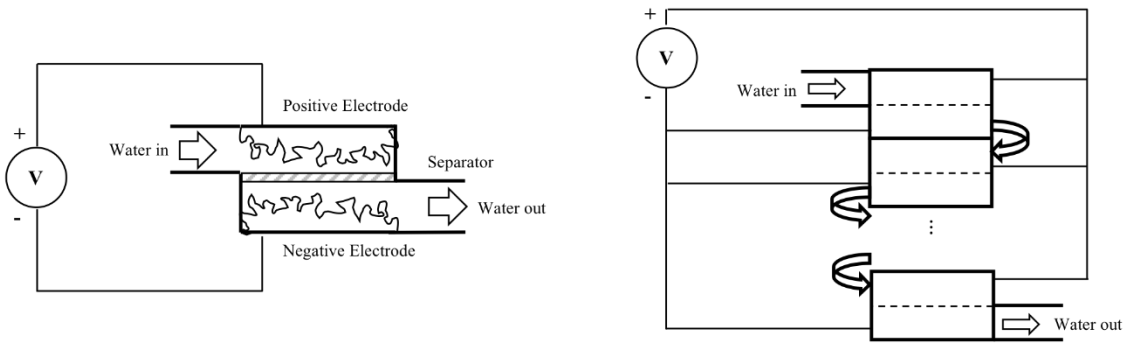

Figure 1: CDI cell (left) and a CDI desalination stack made up of multiple cells (right)

If the EDL capacitance of CDI electrodes in solution is high, a substantial number of ions can be absorbed from feed water, the effect of which can be used to desalinate water. The relationship between electrode capacitance and electro-absorption is approximated by the electrical double layer capacitance formed at the electrolyte and solid interface. If electrode surfaces are considered without electron transfer reactions, Gouy-Chapman-Stern model can be used to estimate the capacitance as two capacitors in series: one at the solid to outer Hemholtz plane, and another due to diffusion in the solution[2]. Oren has estimated that 100g high surface area electrode material (1000m^2/g) can be used to desalinate 1 liter of water at a salt concentration of 3000ppm[2]. Novel materials such as high surface area graphene, along with electrical double layer (EDL) formed by ions near the solid-liquid interface provide high values of capacitance.

Theoretical energy consumption of CDI has been modelled by the following equation from Porada et al.[7,8]:

$$\Delta G = RT\emptyset_{v,fresh}\left(C_{feed} - C_{fresh}\right)\left[\frac{\ln \alpha}{1-\alpha} - \frac{\ln \beta}{1-\beta}\right] \quad (1)$$

where: $\alpha = \frac{C_{feed}}{C_{fresh}}$, $\beta = \frac{C_{feed}}{C_{concentrate}}$, WR (water recovery) $= \frac{C_{concentrate} - C_{feed}}{C_{concentrate} - C_{fresh}}$

For an example of 100mM NaCl brackish water to 5mM NaCl fresh water CDI, if estimate water recovery is 0.8, resulting concentrate is 480 mM NaCl and the desalination energy required is calculated to be 0.12kWh/m^3, which is much lower than energy required for reverse osmosis.

In current literature, there are various units used for salt concentration that are similar in values but differ substantially in concentration or some works mention very low salt concentrations that are two orders of magnitude more pristine than necessary for human consumption[9]. NaCl concentration in units of ppm, typically used in total dissolved solids (TDS) measurement instruments versus mM typically used in laboratory settings is plotted in Figure 2 below. For example, 5ppm is mentioned while 5mM (292ppm) is the taste limit for salt in adults. There is no need to desalinate down to 5ppm when the United States EPA TDS limit for adults is 500ppm[10]. 625ppm is also observed in literature for brackish water while 600mM is seawater. These close values can create confusion for the reader and using ppm is suggested.

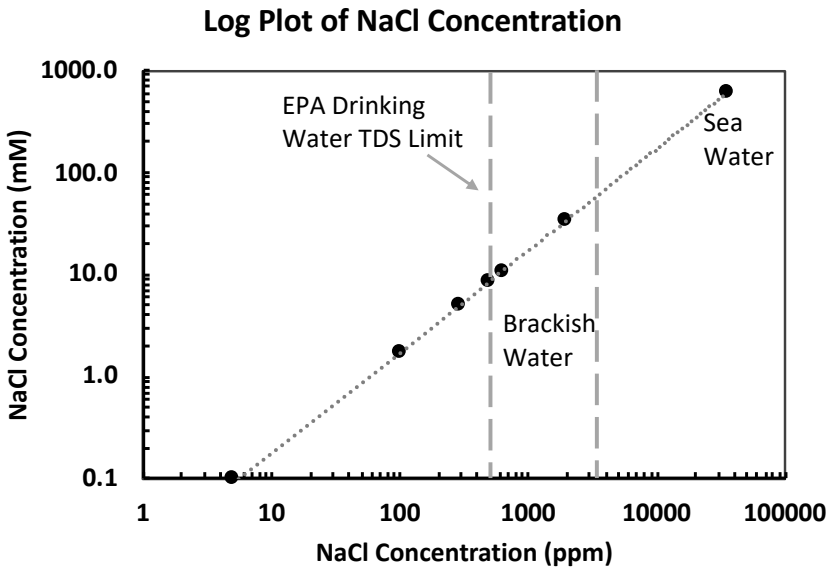

Figure 2: NaCl concentration units and values observed in literature.

2.2 Flow-through versus Flow-by

Water flow for capacitive deionization can be pumped in either flow-through fashion past the electrodes or flow-by in parallel with the electrodes. A direct comparison of these two have been studied in detail by Remillard et al. including with multiple electrode materials to find that flow-by CDI achieved up to 100% more salt absorption capacity[3]. Although the popular flow-through study by Suss et al. report faster absorption rates, Remillard et. al show flow-by is superior in desalination performance when considered holistically[3,11].

Flow-by was chosen in this work for absorption performance, enabling ease of assembly and maintenance by using electrodes on metal substrates. There are four operation modes in a flow-by CDI cell: charging of electrodes to remove ions, pumping forward toward a fresh water reservoir, desorption of ions by discharging the electrodes,

and pumping backward of higher concentrated brine into a reservoir of saltwater. The stages are depicted in Figure 3.

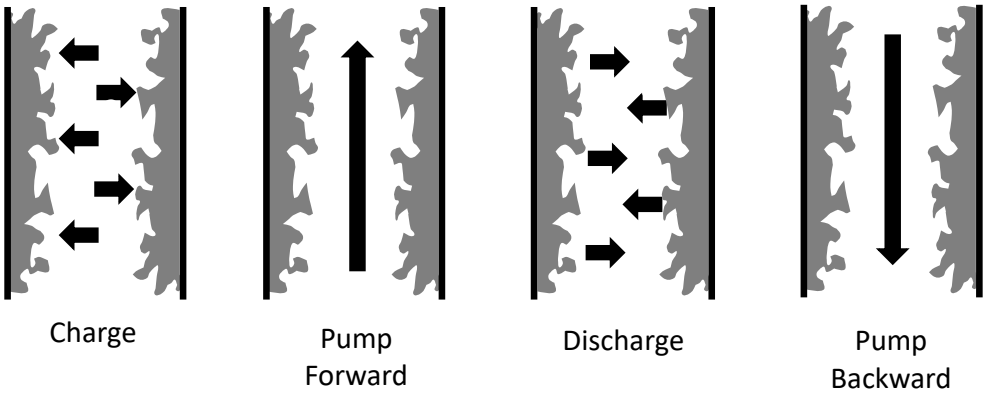

Figure 3: Flow-by operation modes across CDI electrodes

There are difficulties in using the flow-by method with small prototypes as the region with salt concentration gradient is small within one cell. A wider gradient of ion concentration is desired in a flow-by configuration with four-mode pumping system because the amount of water pumped must be of the desired low ion concentration for the product reservoir, and of high concentration to be sent back to the feed reservoir. A stack of CDI cells arranged in a serial fashion would ensure a wider gradient of change between the saline feed input and the fresh water output. Volume of solution within pumps and piping must be less than the amount within the desalination gradient volume to avoid cycling the same already-processed solution within the system.

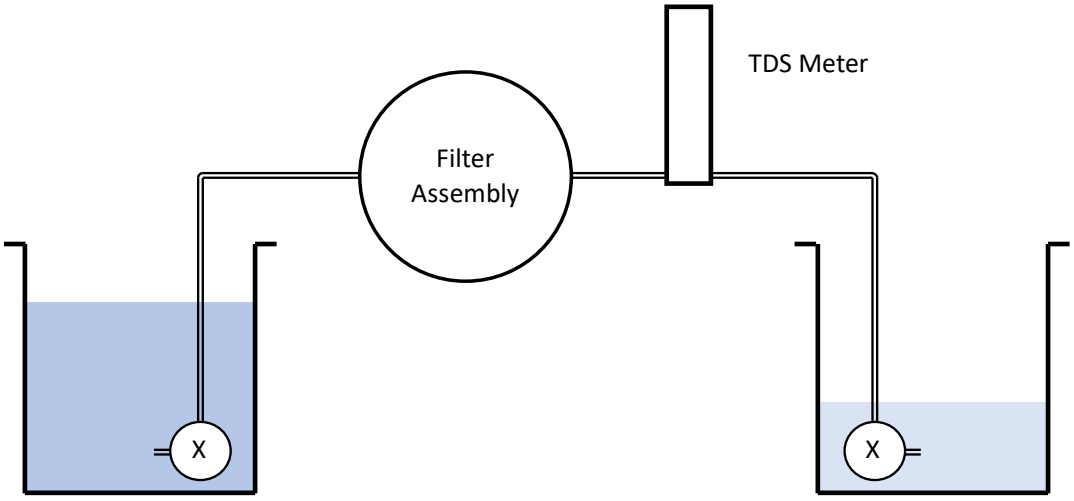

Figure 4: Schematic diagram of a flow-by experimental Setup

2.3 Electrical Circuit Model

With the exception of flow-through electrodes, typical CDI prototypes in prior work make electrical contact with electrodes at the ends of a 2D sheet of material via metal deposition such as gold. However, the bulk electrode resistance contributes to inefficiency which can be shown by SPICE simulations. To model a CDI cell, concatenation of small segments representing material pores which contain fluid can be used. In much of literature, electrical connections are typically connected at the end of material to form electrodes via conductive metal deposition such as with gold. A simple first order electronic circuit model of a basic CDI cell is shown in Figure 5. Rm represents the resistance due to bulk electrode material in a typical prototype system with metal contacts at material ends and Rs represents the solution resistance. For the EDL capacitors to charge and discharge, current must flow through electrode material resistance Rm which reduces the overall efficiency of CDI based water desalination. In

this work, we reduce the effect of electrode material resistance by creating the CDI electrode material directly on a highly conductive, metal substrate.

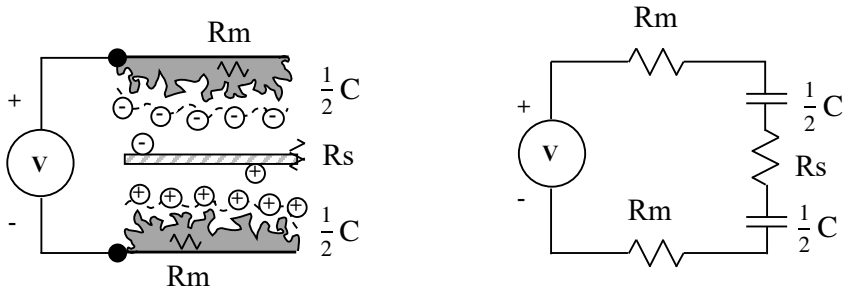

Figure 5: A first order electronic circuit model of a CDI cell.

A single section of a simple CDI circuit model can be analyzed by simplifying it into a half as shown in Figure 6.

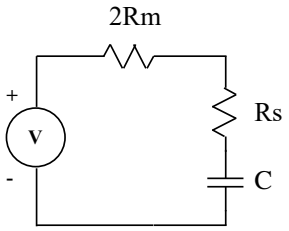

Figure 6: Simplified first order model.

The energy stored on the capacitor is determined by:

$$E = \frac{1}{2} C V^2 \tag{2}$$

where C is the EDL capacitance at one electrode and V is the charge voltage. Note that for the simplified R-C circuit, energy held by the capacitor is independent of

resistances Rm and Rs. However, current necessary to charge and discharge the capacitor passes through these resistors and the series equivalent resistance ($2R_m + R_s$). The energy stored in capacitor C flows through the resistance, causing an equivalent dissipation of energy which is supplied by the source. Similarly, if the supply is replaced by a short after having charged the capacitor, energy in the capacitor in equation (3) will be dissipated by the resistance per the following circuit analysis result for an R-C circuit:

$$E_R = \frac{1}{2} {I_{peak}}^2 R^2 C \tag{3}$$

For the case of $R = (2R_m + R_s)$, this becomes:

$$E_R = \frac{1}{2} {I_{peak}}^2 (2\mathrm{R}_m + \mathrm{R}_s)^2 C \tag{4}$$

which shows that although material resistance R_m is typically small, it still must be minimized for energy dissipated by it is proportional to the square of its value. Series equivalent resistance ($2R_m + R_s$) also determines how fast we can charge and discharge the capacitor.

A lumped element model shown in Figure 7 is a better representation of the bulk electrode with capacitive surface area components. SPICE simulations can be used to depict the effects when multiple segments of electrode models are concatenated as a lumped-element circuit model.

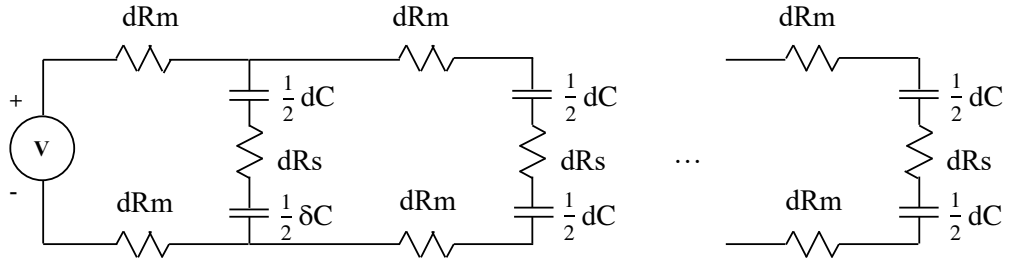

Figure 7: Lumped element model of electrode surface.

As shown in Figure 7, EDL capacitance at further end of an electrode pair located away from the input contacts suffer from the voltage drop due to Rm past each segment. Therefore, the electric field and desalination performance will not be uniform throughout the material. In the simulation below, R_m value of 10 Ohms, R_s value of 1kOhm and capacitance value of 10mF were utilized. SPICE simulation schematic and results in Figure 8 show that for the 10^{th} node in the circuit, the voltage across the double layer capacitance V(node10p)-V(node10n) is 0.6V whereas the first node experiences a voltage differential of 0.9V. Using equation (4) in SPICE circuit simulation, we find that energy stored in capacitance further in bulk material is much less as summarized in Table 1.

Table 1: Summary of energy reduction per node

Node	Differential Voltage	Energy (mJ)	Energy Relative to node1 (%)
1	0.882	4.41	0
2	0.783	3.07	-30.4
3	0.700	2.45	-44.4
10	0.440	0.97	-78.0

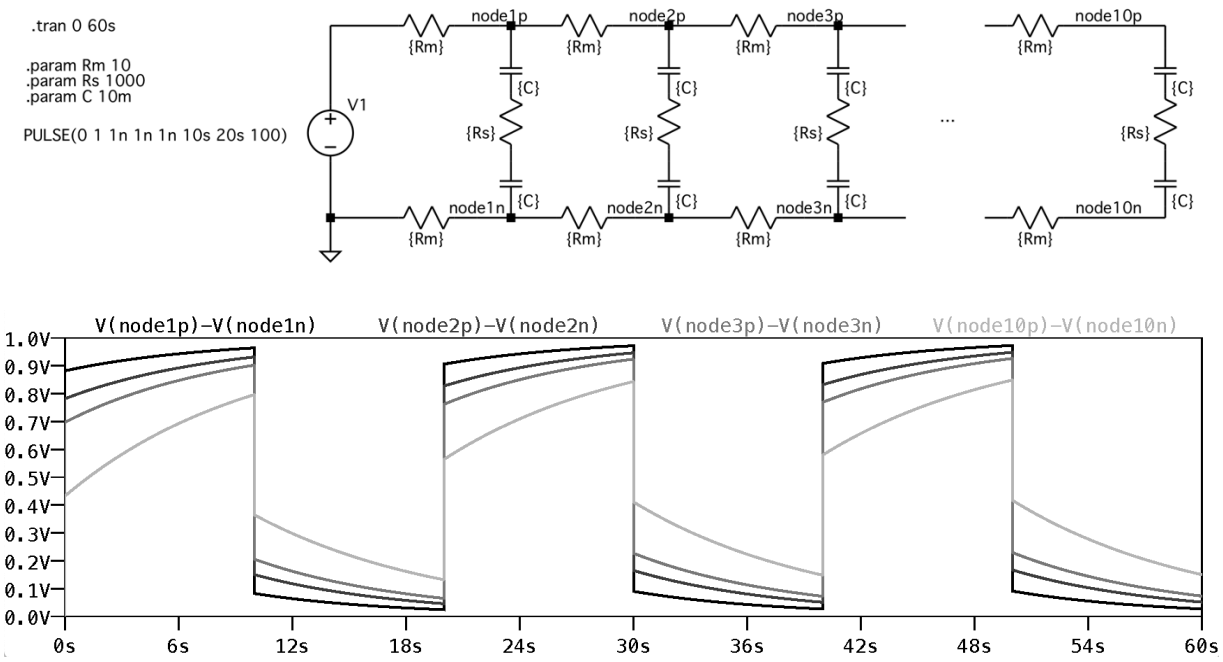

Figure 8: SPICE simulation of lumped element model with schematic and node voltages.

There have been other advancements to increase CDI performance such as by improvements in electrodes by surface topology, the use of ion-selective membranes at the electrodes (referred to as membrane-CDI or MCDI) and energy recovery between charge-discharge cycles[9]. For the purposes of electrode testing, the method of experiments will be kept to a simple CDI cell. Chapter 3 will provide a more detailed look into electrode characteristics.

2.4 EIS Model

Electrochemical impedance spectroscopy is a measurement tool to determine electrochemical properties of an electrode by a low voltage alternating current sweep and

measuring the corresponding changes in sinusoidal current to determine impedance over frequency. Frequencies are typically low from 1mHz up to 100kHz to determine how quickly chemical changes react to the sinusoidal excitation voltage. At the high frequency range, capacitance can be observed, while at low frequencies processes such as diffusion in electrolyte contribute to impedance. Qu et al. have tied CDI electrode EIS measurements to electrical model component values by varying the active material and current collector interface[5]. This enables us to gain insight into CDI electrode performance and use electronics simulation software such as SPICE to study the impact of various electrode physical parameters. It was found that a simple circuit with a resistive element R_S for setup or separator, Q_{CT} (Or C_{CT}) for contact capacitance in parallel with R_{CT} for contract resistance and an electrical transmission line model Z_{EL} can provide a first order model for electrode characteristics[6]. The model of Qu, et al. is similar to the model of Kuo et at. who investigated to isolate component resistance values further. Ku et al. found that the electrical resistances are minimized, most of the power dissipation will be in first the electrode as represented by a transmission line model and second in the separator due to ionic resistance[6].

Using the electrical model and EIS, desired electrical properties of electrode active material can be optimized by iterated manufacturing until EIS measurements agree with models without the need for physical CDI testing. Then, an optimized electrode with these parameters can be fabricated for a CDI cell or stack for a final experimental unit. Thus, CDI electrode performance can be predicted by EIS results, which can itself be predicted by the electronic circuit model as depicted in Figure 9.

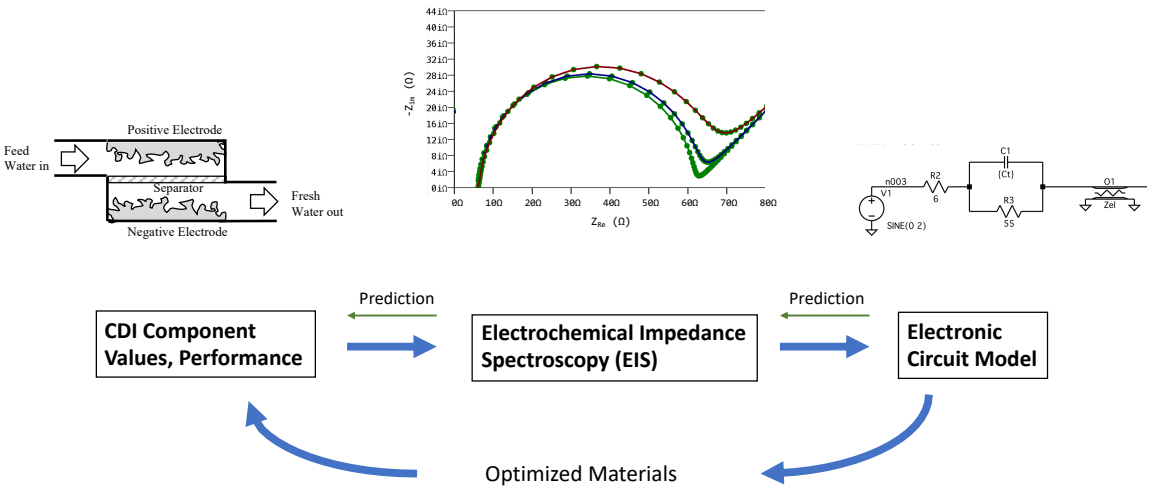

Figure 9: Model and Development Loop Diagram

From EIS data with Nyquist plots of prior work, we can model the electrical circuit elements. For example, from their Nyquist plot, we can estimate that Qu et al. had around 55 Ohms of contact resistance (R_{ct}) by matching circuit model results in Figure 10, which is in close agreement with their text, noting resistance of about 57.2 Ohms[5]. We can also see the effect of a lower resistance contact would have (such as with LIG and Aluminum) on potential EIS data. Real component of impedance moves left as desired. Contact resistance contribution to overall energy consumption can also be estimated as in Figure 11.

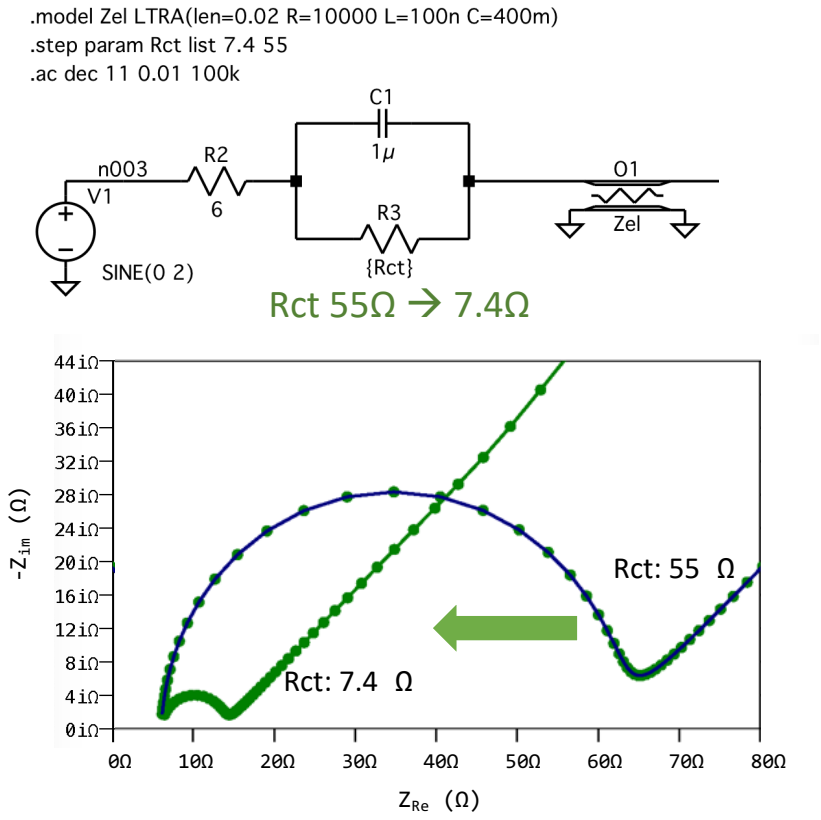

Figure 10: Circuit model for EIS with Nyquist plot from SPICE simulation

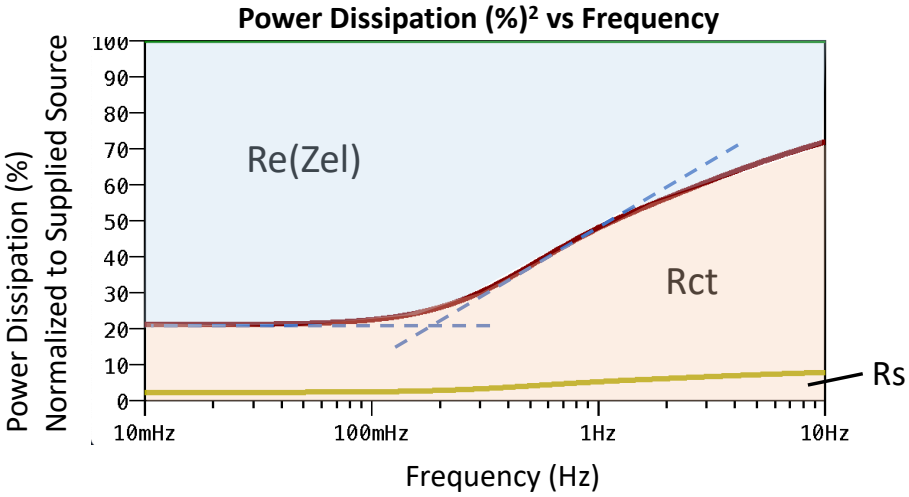

Figure 11: Power Dissipation of Components versus Frequency (bottom)

Percent power dissipation of contact resistnce R_{CT} in EIS electrical model simulation versus overall dissipated power is calculated using the following equation:

$$P_{R_{CT}} = \frac{55\, I(R_{CT})^2}{V_{n003}\, I(V1)\, 100} \tag{5}$$

where the SPICE nodes and variables are in the schematic of Figure 11.

2.5 Limitations

CDI efficiency has been shown to be higher than reverse osmosis (RO) for brackish salt concentrations around 1000 ppm, with a direct relationship between input concentration and energy consumed[2,12]. Qin puts this dependence in terms of electronic charging of a capacitor: as the salt concentration is increased, longer charge times are required to reach a charge voltage[13]. Although the energy dependence on concentration is a limitation which discounts direct seawater desalination of around $30x10^3$ ppm for CDI, brackish water sources or diluted seawater can still be desalinated with high efficiency.

Bio-fouling as well as scaling degrade CDI electrodes by forming a film or covering open pores, resulting in much lower capacitor surface area. In many studies of electrode materials, issues such as bio-fouling have not been adequately addressed. Activated carbon has been a popular low cost high surface area electrode material since early work on CDI by Caudle et al. however activated carbon and more recently aerogel materials are prone to bio-fouling[2,14]. CDI electrode material must ideally be able to avoid bio-fouling or provide an easy mechanism for periodic maintenance to mitigate bio-fouling effects.

Traditional electrodes for CDI as well as batteries or supercapacitors are manufactured using a polymer binder to the active material such as activated carbon (AC) to create a slurry that is applied to a current collector, such as aluminum or copper foil, with controlled thickness via roller compression[15]. A big downside of using binders is the loss of 3D electrode material surface morphology where binder closes pores which then reduces available surface area. CNTs or more typically, carbon black or AC are used. Materials such as AC are more prone to bio-fouling due to the abundance of carbon edges that easily bond with organic molecules. This has posed a challenge for AC for use in desalination since early experiments using it. An ideal material needs to provide good conductivity, keep its high surface area structure after the manufacturing process and repel biofouling and scaling.

Chapter 3

Laser Manufactured Graphene

3.1 Introduction

This chapter describes laser methods considered for high surface area electrode active material manufacturing. The main methods are laser scribed graphene (LSG) and laser induced graphene (LIG). The reasons for selecting laser manufacturing method will also be discussed.

3.2 Laser Scribed Graphene Method

Laser-induced graphene (LIG) is similar to the early laser-scribed graphene (LSG) work done by El-Kady et al. who utilized the infrared laser of an optical LightScribe CD/DVD drive to photothermally reduce graphene-oxide (GO) to graphene[16]. LSG method requires GO synthesis by modified Hummer's method using strong acids and oxidizing agents [16]. LSG electrode manufacturing was considered for CDI electrode manufacturing and found unsuitable in this work. Manufacturing of LightScribe CD/DVD technology is at the end of its consumer life cycle, the drives are hard to purchase and the form factor of electrodes are limited to the disc shape of a CD or DVD. An early prototype with test pattern without graphene electrode of a possible capacitor and a potential CDI cell is shown in Figure 12. It is at this point that the following

challenges became present: (1) electrode current collector connection was found to be an issue as contacts onto thin inter-digitated graphene traces would pose an increase resistance and (2) a separator placed on top of the inter-digitated capacitor sections may not fully isolate positive and negative electrodes due to the small space in-between the inter-digitated pattern. Thus, other graphene manufacturing methods and a way to easily make electrical contact with the electrode is needed.

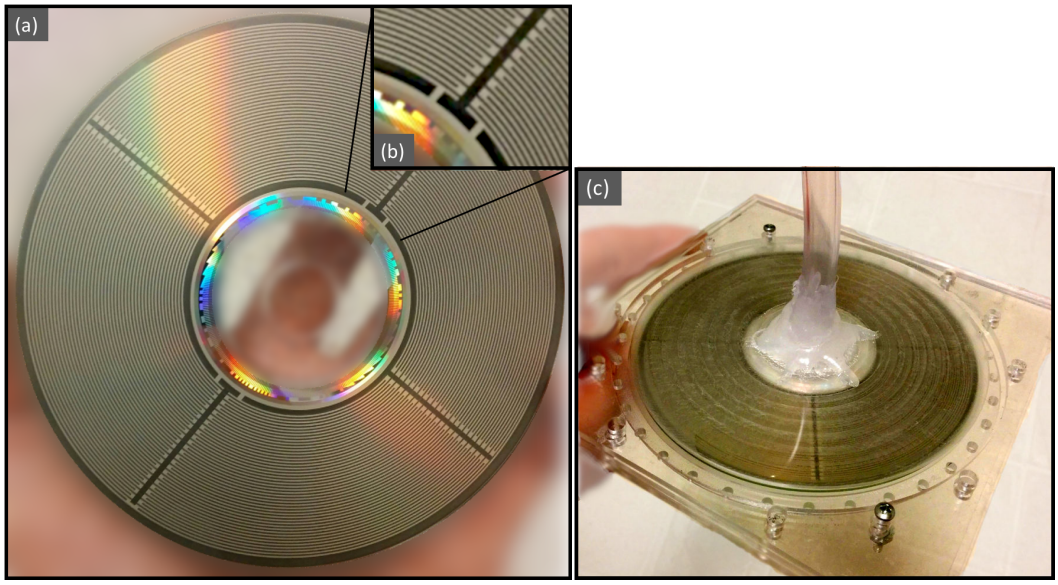

Figure 12: Test prototype of laser pattern (a), zoomed in (b), and cell assembly test using acrylic holder to use with LSG electrode formation from GO (c).

3.3 Laser Induced Graphene Method

An easier approach studied by Ye et al. at Rice University, utilizes infrared laser energy from a common laser cutter machine to process polyimide poly (4,4'-oxydiphenylene-pyromellitimide) (PI) into graphene[17]. This method is referred to as laser-induced graphene (LIG). LIG method can directly process PI into high surface area

graphene with nano-meter scale features. PI is commonly referred to with the industry name of Kapton and can easily be obtained from DuPont de Nemours, Inc. (Wilmington, DE). Alternatively, PI can be made by condensation of pyromellitic dianhydride (PDMA) and 4,4'-oxydiphenylamine (ODA) with ring closure at temperatures up to 300 °C [18]. PI can also be fabricated by ring closure of intermediate polymer poly(pyromellitic dianhydride-co-4,4'-oxydianiline), amic acid (or also referred to as poly(amic acid) (PAA) at 300 °C, depicted in Figure 13, which can be obtained from Sigma-Aldrich (St. Louis, MO) [19].

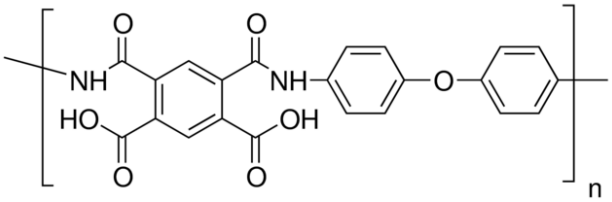

Figure 13: poly(amic acid) (PAA)

After curing in a kiln with a slowly rising temperature profile, solvent evaporation and ring closure is achieved to obtain the following: poly-oxydiphenylene-pyromellitimide or more generally, polyimide (PI) as depicted in Figure 14:

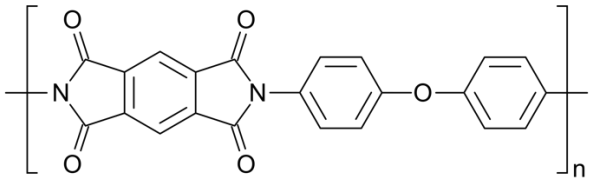

Figure 14: polyimide (PI)

The laser processing step enables a one-step process to turn PI into high surface area and high conductivity graphene by converting sp^3-carbon atoms to sp^2-carbon atoms via photothermal process by infrared laser irradiation[20]. This is illustrated in Figure 15 below. This photo-thermal process is from the highly focused laser providing a local region of high temperature and pressure[20,21]. This extreme environment creates a porous, creased graphene surface with high surface. Ye el al report LIG surface area of about 340 m^2/g that is similar to chemically produced graphene[22,20].

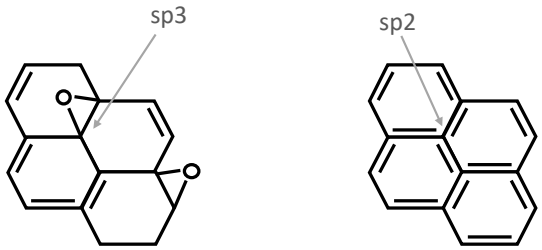

Figure 15: sp^3-carbon and sp^3-carbon atoms

A test sample of Kapton material having undergone infrared laser irradiation to form LIG is show in Figure 16.

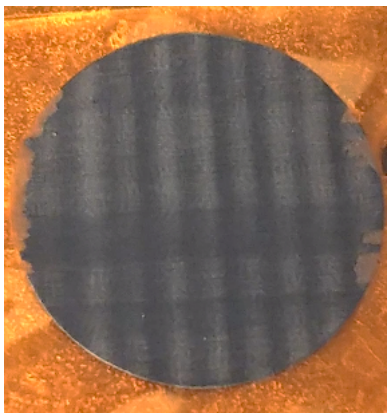

Figure 16: PI after laser irradiation

Ye el al. explored surface characteristics of LIG and were able to adjust the surface water-contact angle via hydrophobic or hydrophilic characteristics of the material by controlling the atmosphere in which laser irradiation is applied[17]. Tittle et al. have reported atmosphere-independent wettability control by adjusting laser power and laser trace spacing as well[23]. The ability to adjust the parameters of the desired graphene product presents an opportunity for high-volume manufacturing of nano-materials with desired properties. For a CDI water desalination application, hydrophilic property is desired in order for water to enter deeper into pores and crevasses of high surface area graphene electrode. Laser irradiation in air and atmospheric pressure are sufficient for this which make the process simple.

Chyan et al. have also shown that LIG can convert a variety of carbon based materials such as coconut shells or bread into high surface area graphene in an inert atmosphere[24]. This presents a potential advantage for LIG of CDI electrodes against bio-fouling by refurbishing them by turning bio-film natural polymers into graphene as part of the electrode.

Chapter 4

Fabrication Method

4.1 Introduction

Fabrication of direct laser-induced graphene (LIG) on metal electrode is detailed below with overall process schematic in Figure 17. A desalination cell is also built to gauge desalination capability.

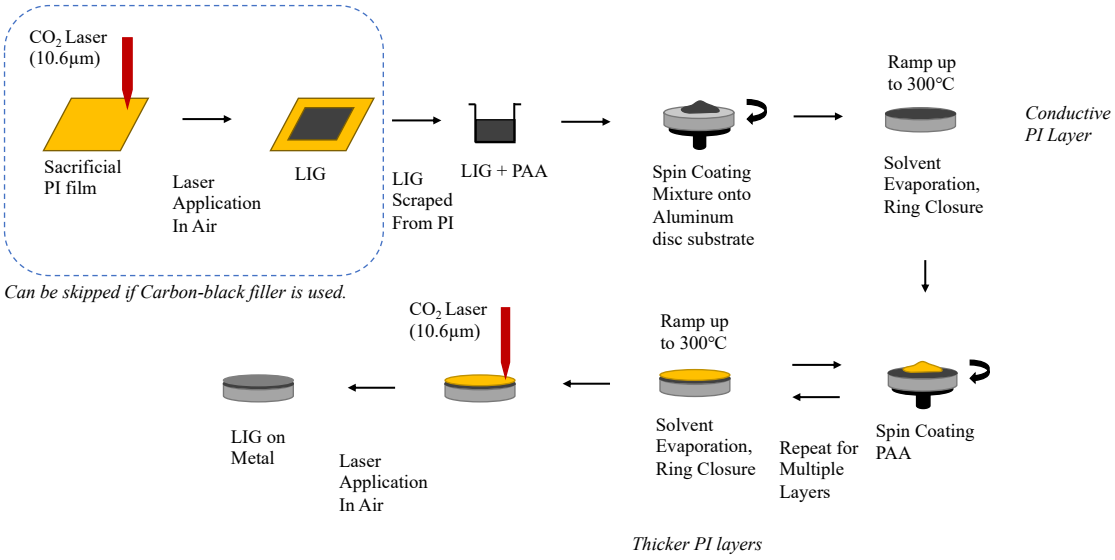

Figure 17: Schematic illustration of the LIG on metal method process

4.2 Direct LIG Fabrication on Metal Substrate

Poly(pyromellitic dianhydride-co-4,4'-oxydianiline) amic acid or also referred to as poly(amic acid) (PAA) was the precursor used for polyimide (PI) from Sigma-Aldrich

(St. Louis, MO). PAA mixed with a conductive additive (Super P carbon 3 % wt.) spin-coated onto 3003 alloy aluminum discs of 50mm in diameter and 3.2mm in thickness (Sharpe Products, New Berlin, WI) as the first conductive later. The conductive additive used was Super P carbon additive (MSE Supplies, Tucson, AZ) but an additional lasering step of sacrificial polyimide (PI) sheet can also be used as detailed in following sections, then the LIG can be scraped off. Super P was chosen as the conductive additive to favor having one less process step.

4.2.1 Spin Coating

Aluminum discs were prepared by cleaning the surface with fine steel wool and alcohol. The first layer of PAA for spin coating needs to contain conductive additive (3% wt.) for it was found that laser processing of only PI did not reach the PI-Al interface. A thin layer of PI was observed on the aluminum surface after scraping away the LIG layer as photographed in Figure 18. It is suspected that Al substrate acts as a heat-sink and the material at the interface does not rise high enough in temperature to turn into graphene.

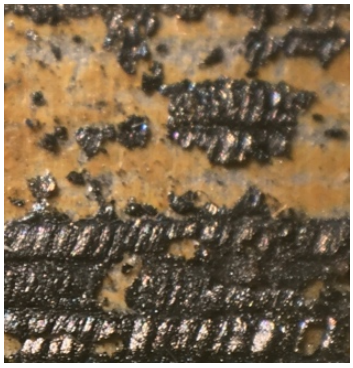

Figure 18: Close up photograph of non-conductive left-over PI on Al surface (orange).

Spin coating speed determines the coated material thickness (t) with the following general equation (6):

$$t \propto \frac{1}{\sqrt{\omega}} \tag{6}$$

More precise equations were published by Meyerhofer in 1978 with or without including the effects of solvent evaporation[25]. For the latter, the equation is as follows:

$$t = \left(\frac{3}{2}\right)^{\frac{1}{3}} k^{\frac{1}{3}} C_0 (1 - C_0)^{-\frac{1}{3}} \rho^{-\frac{1}{3}} \eta_0^{\frac{1}{3}} \omega^{-\frac{1}{2}} \tag{7}$$

where k is a constant specific to the solvent, C_0 is the initial concentration of the solute, ρ is density, η_0 is initial viscosity. Since sample size of produced electrodes did not hinder manual measurement, empirical data with some samples were used to characterize by experimentally adjusting spin speed of coater model VTC200 from MTI Corporation (Richmond, CA) and observing thickness variations as shown in Figure 19. In this spin coating test with 5 test samples per speed, even though the data points show a wide variation, mean thickness values closely match the expected $\omega^{-1/2}$ relationship of equations (6) and (7). Tests up to 10000 rpm were conducted and past 7000 rpm thickness was below 50um and not deemed useful. However higher speeds above 7000 rpm was found useful to remove carbon granules for a more even surface coat. After the upcoming kiln step, additional second layer was coated with only PAA material at slower speed of 2000 rpm in order to obtain a thicker PI base material.

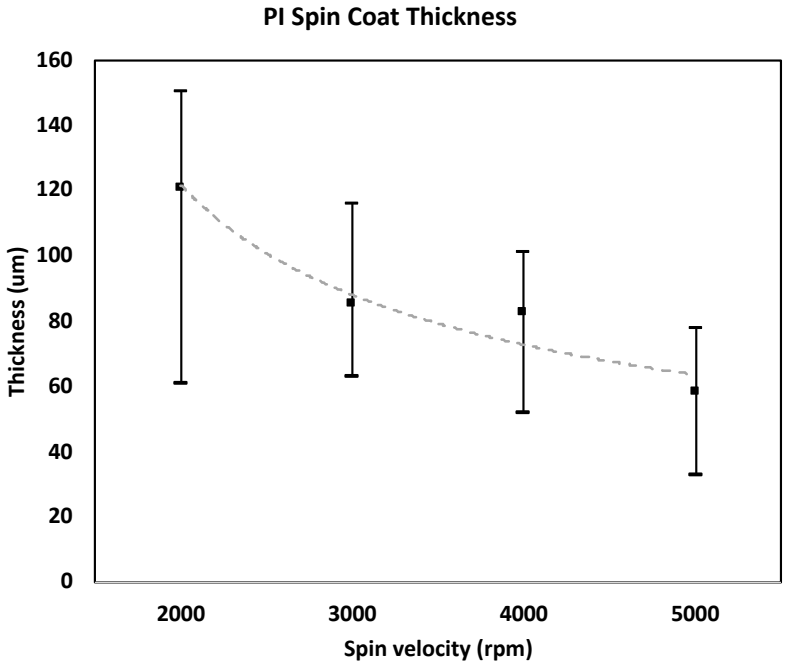

Figure 19: Spin (rpm) versus Thickness (um). Even with variation, $\omega^{-1/2}$ relationship is observed in the trendline.

4.2.2 LIG Conductive Additive

If Super P carbon filler is not desired, conductive filler material can also be prepared by laser irradiation of sacrificial polyimide film that is secured to a temporary substrate (metal or glass) and placed inside a laser cutter commonly found in machine shops or workspaces. To check the feasibility of this, PI sheet of thickness 0.125mm with common name of Kapton HN general-purpose film (DuPont de Nemours, Inc., Delaware) was laser processed to obtain LIG. A 75W CO_2 laser cutter from Universal Laser Systems (Phoenix, AZ) was used to laser irradiate the material with a 10.6μm wavelength to create a 3D porous structure of graphene with high surface area and conductivity[20].

The resulting product is then scraped off with a razor blade. PAA was hand mixed with LIG content of 3 wt. %. After initial testing with LIG, Super P carbon material was used instead due to ease of obtaining the material instead of obtaining from lasering polyimide.

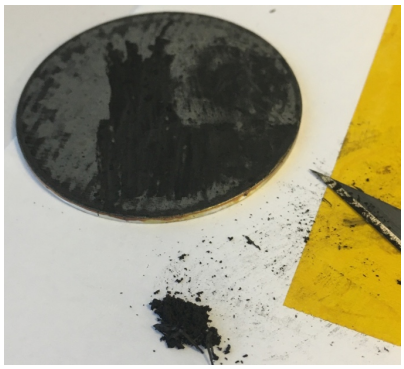

Figure 20: Photograph of scraped LIG material

4.2.3 Kiln Heat Processing

In the next step, the spin coated material on the aluminum metal substrate is step-wise heated over the following temperature profile: 60C/1hr, 120C/1h, 200C/6h, 240 C/ 1h, 325C/1h using a table top kiln, model RapidFire Pro-L from Table Top Furnace Company, LLC (Tacoma, WA).

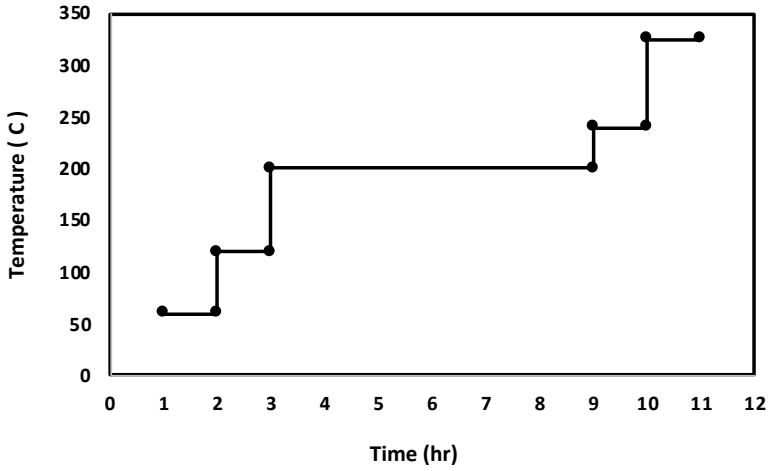

Figure 21: Kiln temperature profile

The initial ramp up is necessary to evaporate NMP solvent which the PAA precursor product includes (15-16% wt.), then 200 C was used instead of 180 C to accelerate imidization and ring closure to form PI. Prior work also indicates that additives into the polymer precursor such as carbon nano-tubes (CNTs) can accelerate imidization for the process is diffusion-limited[26].

4.2.4 Final Laser Processing

Laser setting of 1200DPI made a great impact to improve surface conductivity by a factor of 2. Speed setting was set to 4%, power level at 7% and a z-height of 37mm produced the best result after initial trial of 25 samples. Electrodes were laser irradiated in air to obtain a hydrophilic surface. The resulting electrode is high surface area and conductivity LIG with a thin conductive PI layer to the metal aluminum current collector substrate.

Chapter 5

Results and Discussion

5.1 Introduction

Findings are summarized along with discussion of observations. Comparisons are made to prior work.

5.2 Electrode Resistance Results

Measurements of surface resistance were taken using custom made four-point probe and using a Keysight 34461A precision multi-meter. As observed by Qu et al., four-point probe measurement is correlated with the low frequency portion of the EIS Nyquist plot[5]. Similar to their findings, clamping force was required for a stable measurement. LIG on PI samples were measured to have an average of 48 Ohms sq. resistance. Compared to prior work such as by Ye et al., this is still high since they were able to obtain about 15 Ohms sq. for their material indicating room for improvement. However, when formed on the metal substrate, the lower resistance of current collector aluminum decreased the average resistance to 18 Ohms sq. which is akin to a LIB anode but has the potential to go even lower. Data is summarized in Figure 22 below.

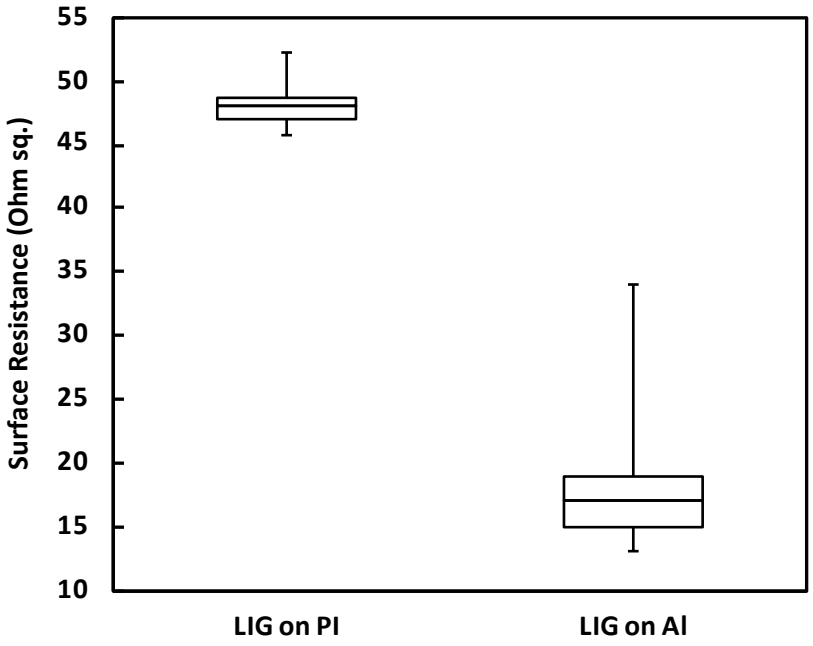

Figure 22: Resistance on PI versus Aluminum substrate

Other methods of using binders with conductive additives are also compared. Hu et al. used CNTs on a stainless-steel current collector and although high frequency measurements are noted, low frequency data from Nyquist plot indicates surface resistance of around 150 Ohms sq., which is an order of magnitude higher than achieved in this work. Lithium-ion battery (LIB) anodes are also manufactured using a binder to attach the common active element graphite onto a copper current collector. Such a battery anode was characterized by An et al. with 92% graphite composition, to have resistance of 20 Ohms sq. after 100 cycles, 100 depth of discharge. Since LIB anodes make up trade secrets of battery manufacturers, measurement data is not commonly available. For this reason, and to confirm the resistance value, an 18650 battery of 2200mAh capacity was

disassembled after 100% discharge and anode measured the same way as all other electrode measurements in this work. The measurement of 19 Ohms sq. is very close to the value Hu et al. found. These findings are summarized in Table 2.

Table 2: Summary of low frequency sheet resistance of various electrodes

Electrode	**Surface Resistance (Ohm sq.)**	**Notes**
CNT film on stainless steel, Hu et al.[27]	~150	Low frequency data from Nyquist plot.
LIB Anode[28]	~20	After 100 cycles, 100% depth of discharge. Major composition: 91.8wt% A12 graphite, 2wt% C-45 carbon, 6wt% PVDF
Li-ion Anode from 2200mAh 18650 Battery (measured)	19	Measured using four-point probe as other samples in this work. Copper current collector.
LIG on PI (Ye et al.)[17]	~15	
LIG on PI (this work)	48	Mediocre LIG, can be tuned further to reach result above.
LIG on PI+Al (this work)	18	Similar to LIB anode but has the potential to get lower.

For a small set of samples, spin coat thickness was varied and resistance measurements were taken for comparison. As expected, due to more conductive material presence, thicker LIG samples resulted in lower resistance as shown in Figure 23. Correlation between surface sheet resistance and through resistance from the electrode surface to aluminum metal side was observed as plotted in Figure 24.

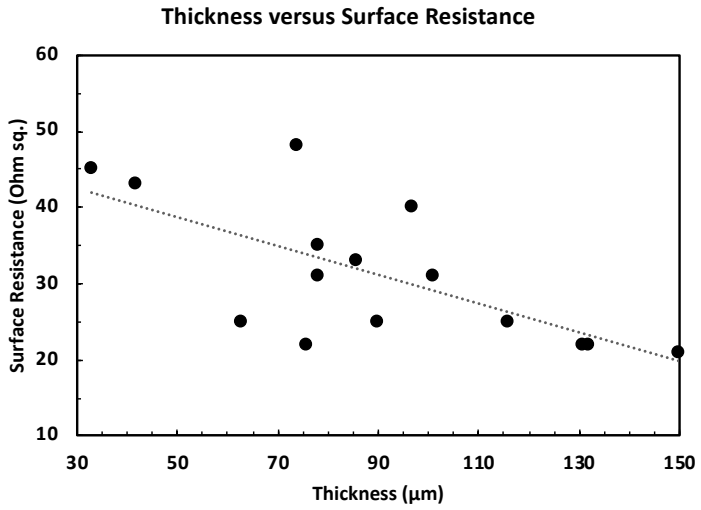

Figure 23: Thickness and resistance comparison

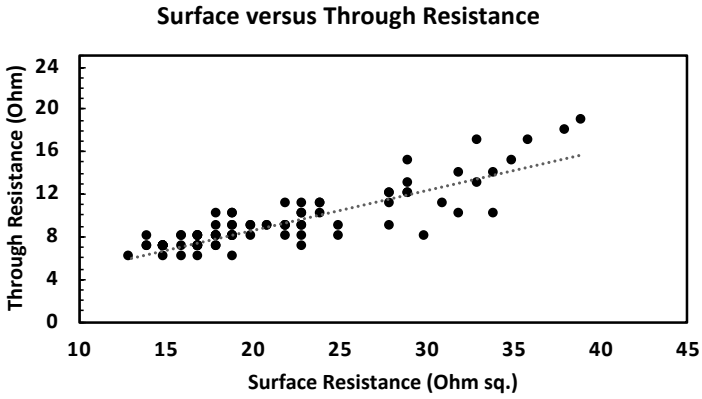

Figure 24: Electrode Sheet Resistance Correlation with Through Resistance to Aluminum Side

5.3 SEM Captures of LIG on Aluminum

SEM equipment of Zeiss Gemini Supra 55 VP-SEM at LLBL Molecular Foundry was used to visualize the surface of produced LIG as captured in Figure 25 and Figure

26. In Figure 25, macro-pores are present with >50nm features that enable ease of access into SEM visible meso-pores (2-50nm). These, along with micro-pores of less than 2nm make up tortuosity for lower ionic resistance.

Cross section SEM capture in Figure 26 shows the high surface area LIG material with open pores for the top surface which interfaces with salt-water at a thickness around 53µm, then the conductive PI layer (with LIG or carbon additive) at about 4µm thickness before aluminum are observed. The conductive PI layer also acts to protect aluminum metal from salt-water corrosion. Other materials may be used instead of aluminum which was only chosen for ease of availability.

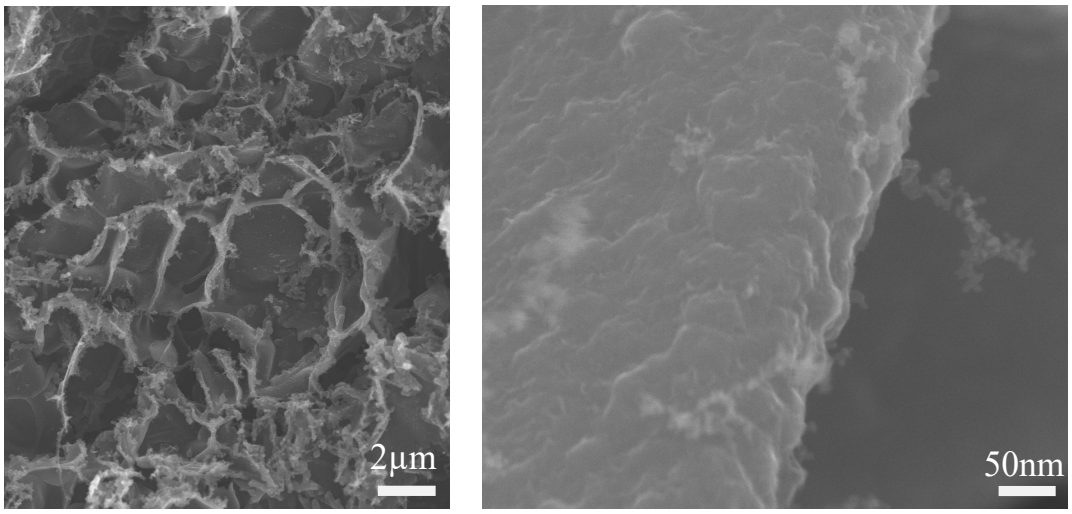

Figure 25: SEM images of LIG surface.

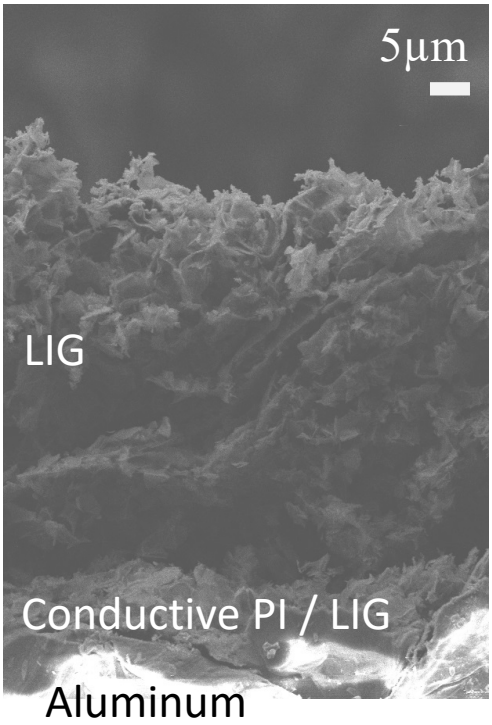

Figure 26: Annotated cross-section SEM image.

5.4 Raman Spectrum

In order to confirm laser irradiation produced few-layer graphene and not amorphous carbon nor many-layer graphene (graphite), Raman spectroscopy was conducted. Using 532nm excitation, Raman shift plot is shown Figure 27.

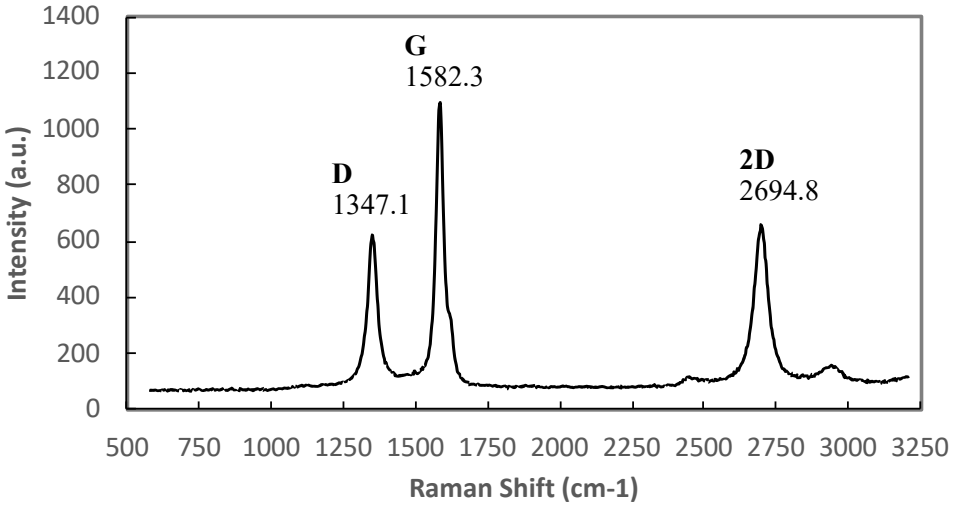

Figure 27: Raman shift.

G band label in Raman spectrum represents graphene in-plane vibration mode for sp^2 hybridized carbon atoms. The D band represents the disorder of sp^2 carbon rings, near the graphene edge. The 2D band, or second order of D band, is of high importance along with the G band for presence of graphene[29]. In comparison, graphite on the other hand has a wide 2D excitation width due to many layers of graphene being stacked on top while LIG spectrum shows a relatively thin 2D peak indicating few-layer graphene. The spectrum is similar to prior work of LIG formation by Chyan, Ye, et al. and confirms the presence of few-layer graphene present in LIG material produced[24].

5.5 CDI Cell

The schematic of a basic CDI cell assembly is shown in Figure 28 and a photograph of the assembly in Figure 29. The two halves are bolted together at four points with a gasket in between. Assembled filter assembly was filled with 1210ppm

concentration of saline solution from a mixture of NaCl and DI water. Leaks were common during initial assembly and silicone was used along with rubber gasket in between the two halves.

Capacitance measurement of the electrodes was out of the range of available equipment, Keysight 34461A 6.5 Digit Multimeter (Santa Rosa, CA), so an analytical approach was used to solve for the relatively high capacitance value. First, direct-current resistance across the electrodes was measured to be 6.3kOhms. Then, the capacitor assembly consisting of electrodes, saline solution as an electrolyte, and polypropylene separators making up the cell stack was charged to 1.2V using a lab bench power supply, then disconnected while measuring the time of self-discharge down to the arbitrary value of 0.72V within 37.88 seconds. This R-C circuit voltage decay was simulated on SPICE to solve for capacitance, obtaining the result of 11.8mF.

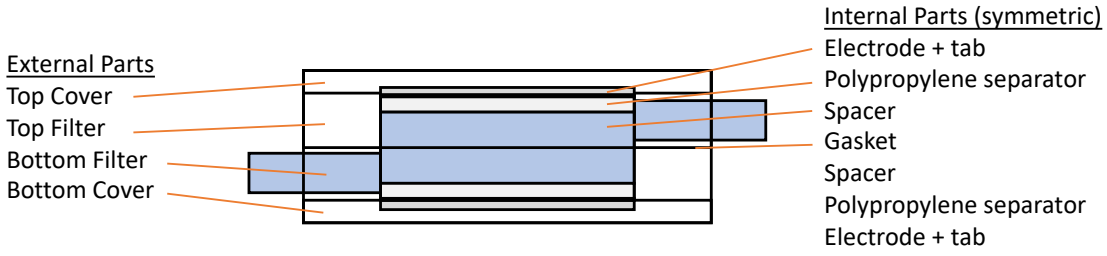

Figure 28: CDI cell schematic.

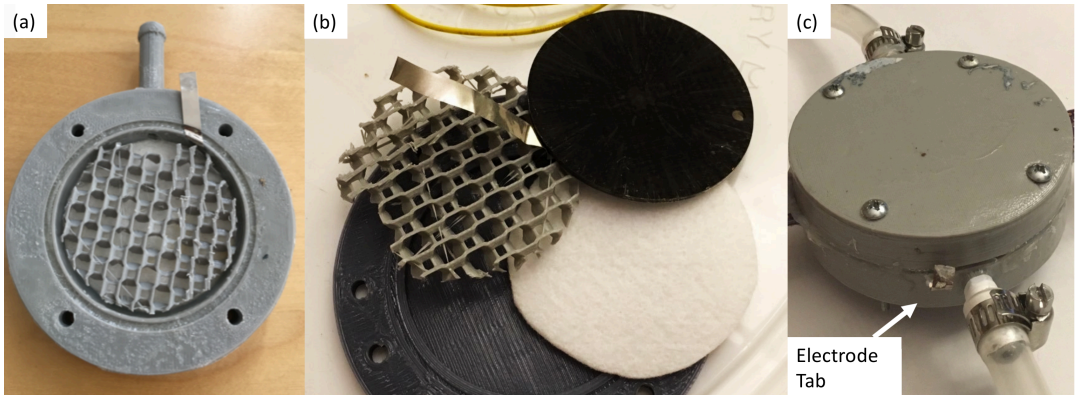

Figure 29: Photographs of (a) half-cell, (b) components and (c) full assembly.

Electrodes were charged to 1.2V using an electro-mechanical relay controlled by a micro-controller (Arduino Uno) and TDS measurements captured along with electrode voltage as plotted in Figure 30. When charged, sodium and chloride ions get adsorbed in the electrode and TDS measurement dips to about 1110ppm for a reduction of 8.3%, showing desalination of brackish water with a simple CDI cell using LIG on aluminum substrate.

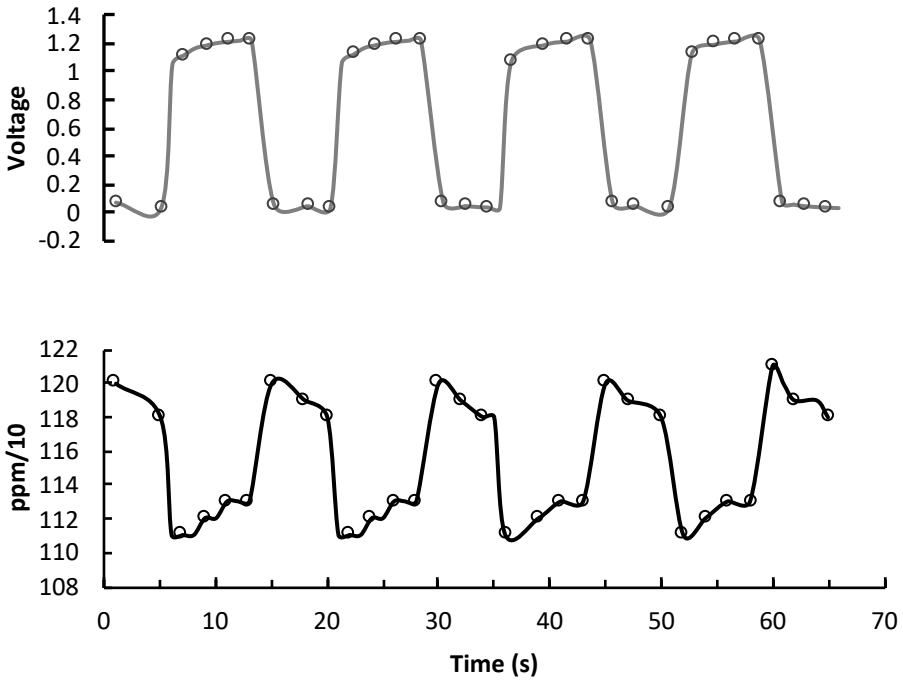

Figure 30: Time series showing application of voltage reduces NaCl concentration.

The TDS meter was placed about 10cm away from the cell. The four stages of flow-by CDI mean that water must be pumped into the fresh reservoir on average. Running the system for 2 hours showed small difference between salt concentration measurements of the two reservoirs which means that fresh water was getting mixed with higher concentration water within the tubes. A valve, M-CDI, or an experimental setup with many cells making up a higher volume stack with desalination volume much higher than volume of liquid contained in tubing would enable better feed water and fresh water separation. The issue of concentration gradient in a low volume CDI cell experimental setup is depicted in Figure 31.

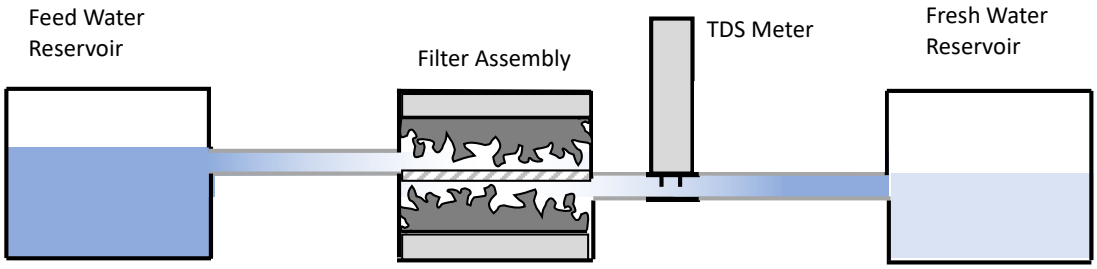

Figure 31: Illustration of salt concentration gradient with a small CDI cell

Chapter 6

Conclusion and Future Work

6.1 Conclusion

In this work, CDI power consumption in the electrode material bulk resistance was improved by making a better electrical contact between metal current collector and the high surface area active material of laser induced graphene. Sheet resistance similar to lithium-ion battery anodes was achieved but one that can hold larger sodium and chloride ions. The electrode active material was formed directly on a metal substrate using a film of conductive PAA which was then converted to PI at a desired thickness and laser irradiated to obtain LIG with high conductivity. The remining thin layer of conductive PI between aluminum and LIG also serves as a binder reducing the need for additional materials. The disclosed fabrication method is roll to roll manufacturing to produce high volumes of electrode materials similar to battery production. The possibility of refurbishing bio-fouled electrodes is also suggested by support of similar work, but remains to be tested. CDI desalination of brackish water is verified.

6.2 Future Work

LIG quality can further be improved to achieve sheet resistance on PI itself of 15 Ohms sq. similar to the results of Ye et al. Then, the LIG on metal fabrication method can

be repeated which will result in a lower overall electrode resistance, further enabling more efficient CDI desalination.

LIG fabrication from PI polymers should be studied to measure outgassing contents such as CO, CO_2, NO_x or any toxic material formation during the laser application process. Any toxic mineral formation can negatively impact the desalinated water and would have to be filtered out.

A single CDI cell is difficult to obtain efficiency or volume desalination figures, so a CDI stack of multiple cells must be produced as a scaled-up experiment next. Issues due to tube water volume and concentration gradients would be at a minimum.

Refurbishing of used electrodes with bio-fouling by reapplication of laser on these natural polymers into additional graphene is highly recommended for future work.

Bibliography

1. Metke, T., Westover, A. S., Carter, R., Oakes, L., Douglas, A. & Pint, C. L. Particulate-free porous silicon networks for efficient capacitive deionization water desalination. *Scientific Reports* **6**, 24680 (2016).

2. Oren, Y. Capacitive deionization (CDI) for desalination and water treatment — past, present and future (a review). *Desalination* **228**, 10–29 (2008).

3. Remillard, E. M., Shocron, A. N., Rahill, J., Suss, M. E. & Vecitis, C. D. A direct comparison of flow-by and flow-through capacitive deionization. *Desalination* **444**, 169–177 (2018).

4. Hesjedal, T. Continuous roll-to-roll growth of graphene films by chemical vapor deposition. *Appl. Phys. Lett.* **98**, 133106 (2011).

5. Qu, Y., Baumann, T. F., Santiago, J. G. & Stadermann, M. Characterization of Resistances of a Capacitive Deionization System. *Environ. Sci. Technol.* **49**, 9699–9706 (2015).

6. Kuo, H. A., Ramachandran, A., Oyarzun, D. I., Clevenger, E. C., Santiago, J. G., Stadermann, M., Campbell, P. G. & Hawks, S. A. Understanding resistances in capacitive deionization devices. *Environ. Sci.: Water Res. Technol.* **6**, 1842–1854 (2020).

7. by Electrodialysis, D. *JR Wilson, Editor*. (Butterworths Scientific Publications, London, 1960).

8. Biesheuvel, P. M. Thermodynamic cycle analysis for capacitive deionization. *Journal of Colloid and Interface Science* **332**, 258–264 (2009).

9. Porada, S., Zhang, L. & Dykstra, J. E. Energy consumption in membrane capacitive deionization and comparison with reverse osmosis. *Desalination* **488**, 114383 (2020).

10. Ziolkowska, J. Desalination leaders in the global market _ current trends and future perspectives. *Water Science & Technology: Water Supply* **16**, 563–578 (2016).

11. Suss, M. E., Baumann, T. F., Bourcier, W. L., Spadaccini, C. M., Rose, K. A., Santiago, J. G. & Stadermann, M. Capacitive desalination with flow-through electrodes. *Energy Environ. Sci.* **5**, 9511–9519 (2012).

12. Qin, M., Deshmukh, A., Epsztein, R., Patel, S. K., Owoseni, O. M., Walker, W. S. & Elimelech, M. Comparison of energy consumption in desalination by capacitive deionization and reverse osmosis. *Desalination* **455**, 100–114 (2019).

13. Qin, M., Deshmukh, A., Epsztein, R., Patel, S. K., Owoseni, O. M., Walker, W. S. & Elimelech, M. Comparison of energy consumption in desalination by capacitive deionization and reverse osmosis. *Desalination* **455**, 100–114 (2019).

14. Yang, C.-M., Choi, W.-H., Na, B.-K., Cho, B. W. & Cho, W. I. Capacitive deionization of NaCl solution with carbon aerogel-silicagel composite electrodes. *Desalination* **174**, 125–133 (2005).

15. Choi, J.-Y. & Choi, J.-H. A carbon electrode fabricated using a poly(vinylidene fluoride) binder controlled the Faradaic reaction of carbon powder. *Journal of Industrial and Engineering Chemistry* **16**, 401–405 (2010).

16. El-Kady, M. F., Strong, V., Dubin, S. & Kaner, R. B. Laser Scribing of High-Performance and Flexible Graphene-Based Electrochemical Capacitors. *Science* **335**, 1326–1330 (2012).

17. Ye, R., James, D. K. & Tour, J. M. Laser-Induced Graphene. *Acc. Chem. Res.* **51**, 1609–1620 (2018).

18. Bryant, R. G. Polyimides. in *Ullmann's Encyclopedia of Industrial Chemistry* 1–27 (American Cancer Society, 2014). doi:10.1002/14356007.a21_253.pub2.

19. Ha, Y., Choi, M.-C., Jo, N., Kim, I., Ha, C.-S., Han, D., Han, S. & Han, M. Polyimide multilayer thin films prepared via spin coating from poly(amic acid) and poly(amic acid) ammonium salt. *Macromol. Res.* **16**, 725–733 (2008).

20. Lin, J., Peng, Z., Liu, Y., Ruiz-Zepeda, F., Ye, R., Samuel, E. L. G., Yacaman, M. J., Yakobson, B. I. & Tour, J. M. Laser-induced porous graphene films from commercial polymers. *Nat Commun* **5**, 5714 (2014).

21. Dong, Y., Rismiller, S. C. & Lin, J. Molecular dynamic simulation of layered graphene clusters formation from polyimides under extreme conditions. *Carbon* **104**, 47–55 (2016).

22. Ye, R., Liu, Y., Peng, Z., Wang, T., Jalilov, A. S., Yakobson, B. I., Wei, S.-H. & Tour, J. M. High Performance Electrocatalytic Reaction of Hydrogen and Oxygen on Ruthenium Nanoclusters. *ACS Appl. Mater. Interfaces* **9**, 3785–3791 (2017).

23. Tittle, C. M., Yilman, D., Pope, M. A. & Backhouse, C. J. Robust Superhydrophobic Laser-Induced Graphene for Desalination Applications. *Adv. Mater. Technol.* **3**, 1700207 (2018).

24. Chyan, Y., Ye, R., Li, Y., Singh, S. P., Arnusch, C. J. & Tour, J. M. Laser-Induced Graphene by Multiple Lasing: Toward Electronics on Cloth, Paper, and Food. *ACS Nano* **12**, 2176–2183 (2018).

25. Meyerhofer, D. Characteristics of resist films produced by spinning. *Journal of Applied Physics* **49**, 3993–3997 (1978).

26. Tang, Q.-Y., Chen, J., Chan, Y. C. & Chung, C. Y. Effect of carbon nanotubes and their dispersion on thermal curing of polyimide precursors. *Polymer Degradation and Stability* **95**, 1672–1678 (2010).

27. Hu, L., Wu, H., La Mantia, F., Yang, Y. & Cui, Y. Thin, Flexible Secondary Li-Ion Paper Batteries. *ACS Nano* **4**, 5843–5848 (2010).

28. An, S. J., Li, J., Mohanty, D., Daniel, C., Polzin, B. J., Croy, J. R., E. Trask, S. & Wood, D. L. Correlation of Electrolyte Volume and Electrochemical Performance in Lithium-Ion Pouch Cells with Graphite Anodes and NMC532 Cathodes. *J. Electrochem. Soc.* **164**, A1195–A1202 (2017).

29. Ferrari, A. C., Meyer, J. C., Scardaci, V., Casiraghi, C., Lazzeri, M., Mauri, F., Piscanec, S., Jiang, D., Novoselov, K. S., Roth, S., & others. Raman spectrum of graphene and graphene layers. *Physical review letters* **97**, 187401 (2006).